

**B₃₆ bowl-like nanostructure as candidate for carrier of
sulfonamide molecule: A theoretical study**

Saeedeh Kamalinahad^{a*}, Azim Soltanabadi^b and Pablo Gamallo^c

^a Young Researcher and Elite Club, Arak Branch, Islamic Azad University, Arak, Iran

^b Department of Physical Chemistry, Faculty of Chemistry, Razi University,
Kermanshah, Iran

^c Departament de Ciència de Materials i Química Física & Institut de Química Teòrica
I Computacional (IQTUCB), Universitat de Barcelona, c/ Martí i Franquès 1-11, 08028,
Barcelona, Spain

* To whom correspondence should be addressed. Email: saedehkamalinahad@gmail.com

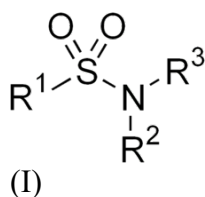
Abstract

Density functional theory (DFT) method used to investigate interaction of sulfonamide with the B₃₆ nanocluster. The obtained results indicate that although sulfonamide weakly interacts with convex and concave sides of nanocluster, the B atom at the edge of B₃₆ nanocluster is favorable position for adsorb sulfonamide via oxygen atom. The interactions are also studied in terms of NBO charges analysis. The electronic properties of nanocluster are significantly altered after adsorption sulfonamide molecule. The energy gap of the stable system is reduced which could be applied as a chemical signal. Indeed, it is found that the adsorption of sulfonamide molecule at the edge of the B₃₆ nanocluster is effective in water medium. The relative high dipole moments are estimated for B₃₆/sulfonamide configuration, exhibiting that these systems could be solubilized or dispersed in polar mediums, like water. The obtained results introduce the B₃₆ nanocluster as an efficient carrier for delivery of sulfonamide in nanomedicine domain.

Introduction:

Sulfonamide (SA) is a functional group (a part of a molecule) that is the basis of several groups of drugs, which are called sulphonamides, sulfa drugs or sulpha drugs. Sulfonamides are the first successfully synthesized selectively toxic antimicrobial drugs [1,2]. Sulfonamides with the antimicrobial activity represent a large group of drugs which can be classified in different ways. One of the most comprehensive is the sulfonamides classification [3] into: Oral sulfonamides which can be absorbed, oral sulfonamides which cannot be absorbed and topical sulfonamides. Several drugs containing sulfonamide functionality are in clinical use which include antibacterial and antifungal drugs [4,5], carbonic anhydrase inhibitors [6,7], anti-inflammatory agents [8], anticonvulsant agents [9], antimigraine agents [10], hypoglycemic, protease inhibitors [11] and agents acting against diabetic mellitus [12]. They are also found to have extensive applications in cancer chemotherapy [13,14].

Sulfonamides are compounds, which have a general structure represented by **I**. In this structure, R^1 may be alkyl, aryl or hetero aryl etc. R^2 , R^3 may be hydrogen, alkyl, aryl or hetero aryl groups. After sulfanilamide discovery, thousands of chemical variations were studied and the best therapeutic results were obtained from the compounds in which one hydrogen of the SO_2NH_2 group was replaced by heterocyclic ring [15]. To date more than twenty thousand sulfanilamide derivatives, analogs and related compounds have been synthesized. These syntheses have resulted in the discovery of new compounds with varying pharmacological properties [15].



The application of nanotechnology in disease treatment, diagnosis, monitoring, and in the control of biological systems at the single molecule or molecular assembly level is referred to as nanomedicine because of their novel properties as well as extreme different functionality compared to their bulk counterparts. The major goal of nanomedicine is the design of material capable of delivery and targeting of pharmaceutical, therapeutic, and diagnostic agents. Since the mid-1980s, the development of nanocarriers, incorporating receptors specific for the target cells, has certainly been the most promising strategy. The use of nanostructures as nanomedicine has been investigated both theoretically and

experimentally [16-22].

After the discovery carbon nanostructures [23,24] analogous boron nanostructures were interested [25-27]. Boron is an electron deficient element which has a rather fascinating chemistry [28]. In contrast to the covalent, ionic, van der Waals, and metallic bonds, it has a variety of crystal structures containing multicenter bonds, which is a result of an electron deficiency [29,30]. Boron is possibly the second element that can possess multiple low-dimensional allotropes. Indeed, previous theoretical predictions by Boustani [31,32] suggested that small-sized boron clusters exhibit quasi-planar structures, which were later confirmed experimentally by Wang, Boldyrev, and their co-workers [33-35]. Recently, the quasiplanar boron clusters (B_{36}) with sixfold symmetry and a central hexagonal hole has been synthesized [36]. The strongly bound atoms of B_{36} enhance its resistance to mechanical impact. This nanostructure has potential to have an important role in future thin film technology and two-dimensional materials research. These structures can serve as potential chemical sensors [37], hydrogen storage [38], electro-optics [39] and carrier for drug delivery [40]. In this study, we investigated the ability of B_{36} nanocluster to adsorb sulfonamide molecule (SA) as a promising nanocarrier with quantum chemical research. Up to now, based on our knowledge, this is the first report of the use of B_{36} nanocluster as a sulfonamide nanocarrier. The results may provide a new insight to the development of nanomedicine domain.

Computational details

The geometries of B_{36} nanocluster, sulfonamide molecule and SA/ B_{36} configuration are fully optimized at M06-2X/6-31G(d,p) level of theory and the nature of the stationary points are checked by frequency analysis at the same computational level. The correlated $\langle S^2 \rangle$ values are zero, which confirms the pure singlet states. The M06-2X functional could be a high non-locality functional with double the amount of non-local exchange (2X) to ponder dispersion forces [41]. The hybrid M06-2X functional has been applied as an acceptable method in many nano scale molecular systems due to the higher percentage of Hartree-Fock exchange (54%) [42,43]. In order to analyze the solvation effects on the stabilities of the studied complexes, solution effects were investigated using the polarizable continuum model (PCM) [44,45] with dielectric constant of 78.3553 for water at the M06-2X/6-31G(d,p) level of

theory. The charge polarization between B₃₆ and the SA molecule was calculated by using natural bond orbitals (NBO) analysis [46]. All calculation was performed using Gaussian09 package [47].

Energy gap (E_g), Fermi level energy (E_F), and adsorption energy (E_{ads}) values as quantum molecular descriptors [48] were computed. The energy gap has the following operational equation:

$$E_g = (E_{LUMO} - E_{HOMO}) \quad (1)$$

In this definition, E_{HOMO} and E_{LUMO} are the energy of highest occupied and lowest unoccupied molecular orbitals, respectively. The conventional assumption for the Fermi level energy (E_F) is that it reclines approximately in the middle of the energy gap (E_g) at 0 K.

The adsorption energy (E_{ads}) of sulfonamide over the surface of pristine B₃₆ is defined as,

$$E_{ads} = E_{complex} - E_{SA} - E_{B_{36}} \quad (2)$$

Where $E_{complex}$, E_{SA} and $E_{B_{36}}$ are total energies of B₃₆/SA configuration, isolated sulfonamide, and pristine B₃₆ nanocluster, respectively. According to the Eq. (2), negative adsorption energy correlates to the stability of interacting complex.

Total density of states (TDOS) analysis were performed on the pristine fragments and B₃₆/SA complex at the same level of theory using the GaussSum program [49].

RDG was also used hereto characterize the non-covalent interactions. The dimensionless RDG (s) is evaluated from the density (ρ) and its first derivative [50], $RDG = (1 / (2(3\pi^2)^{1/3})) ((|\nabla\rho|) / \rho^{4/3})$. Density values give just information about the strength of interaction and not provide clear classification of them as attractive or repulsive. For this purpose, the sign of the second eigenvalue (λ_2) of the electron density Hessian matrix is considered to distinguish between different types of non-covalent interactions, i.e., hydrogen

bonding, van der Waals interaction, and steric repulsion. So, electron density increased with λ_2 sign, is used as a descriptor for the nature of interacting bonds; $\Omega = \text{sign}(\lambda_2)\rho$. MULTIWFN [51] software was used here to draw the non-covalent interaction (NCI) plots, RDG versus $\text{sign}(\lambda_2)\rho$. Low-density and low-gradient spikes associated with density located between interacting paths are as signature of non-covalent interactions.

Results and Discussions

Geometry optimization and structure of pristine B₃₆ nanocluster in gas phase and water medium

The optimized structures of pristine B₃₆ and sulfonamide at the M06-2X/6-31G(d,p) level of theory in the gas phase are shown in Fig. 1a and 1b. It is observed that the B₃₆ nanocluster has bowl shape with a central hexagonal hole. This structure has different kinds of B-B bonds. Some of the bond lengths are shown in this figure. Also, we take a look at the frontier molecular orbital energies (E_{HOMO} and E_{LUMO}) and E_g values for the considered nanocluster, listed in Table 1. The obtained energy gap quantity for the B₃₆ is about 3.42 eV. Moreover, TDOS and graphic presentation of the HOMO and LUMO distribution for B₃₆ nanocluster are presented in Fig. 1c.

In the next step, investigation of the solution effects on the adsorption molecule is in order. The optimization procedure for B₃₆ and sulfonamide is done with imposing polarizable continuum model (PCM) in water medium, and their structures are shown in Fig. 2a and b. As inferred from Fig. 2a, there is no clear difference between the bond lengths in the gas phase and water medium. The electronic properties of this nanocluster are also listed in Table 1. The value of energy gap for B₃₆ is observed about 3.43 eV which is slightly increased with respect to the corresponding quantities in the gas phase. TDOS and graphic presentation of the HOMO and LUMO distribution of pristine B₃₆ in water medium were presented in Fig. 2c.

Sulfonamide Adsorption on Pristine B₃₆ nanocluster in Gas Phase and Water Medium

In order to obtain stable configurations of the adsorbed sulfonamide (SA) molecule on the convex and concave surfaces of the B₃₆ nanocluster different possible adsorption structures were examined. The electrostatic potential (ESP) distribution has been widely used to determine electrophilic and nucleophilic sites. The regions with low ESP are characterized by the negative charge and are shown in red color in a typical ESP map. Conversely, the regions with high ESP, the positive charge, are shown with blue color (see Fig. 1d). It can be seen that the electron density (red color in Fig. 1d) is localized on the O atoms of sulfonamide. Thus, sulfonamide can be approach to the nanocluster by the O atom.

In this section, we have searched for appropriate configuration of the adsorb SA on the B₃₆ nanocluster in gas phase. After full optimization of various initial structures, eight stable adsorption configurations are obtained. These relaxed structures and their corresponding binding distances are given in Fig. 3 and S1. The calculated E_{ads} values for these configurations are listed in Table 2 and S2. According to the results of these tables, E_{ads} values for these configurations are between -37.79 to -64.74 kJ/mol. Among them, B₃₆/SA configuration implies the strong physisorption process of SA molecule onto B₃₆ surface by appreciable adsorption energies. Actually, the SA molecule do not adsorbed efficiently on the both convex and concave surfaces of the B₃₆ nanocluster through these configurations. This claim is confirmed by great interaction distances (2.5-3.5 Å) and small E_{ads} (see Fig. S1 and Table S2). In the most stable configuration (B₃₆/SA), the oxygen atom of sulfonamide (the negative region in the ESP map) approaches the B atom at the edge of B₃₆ nanocluster with an interaction distance of 1.532 Å and $E_{\text{ads}} = -64.74$ kJ/mol. It seems that the boron atoms at the edge of B₃₆ are more reactive toward the nucleophilic attacks of the SA molecule. It is noticeable that the B₃₆ nanocluster significantly distorts at the adsorption site. The deformation is obviously observed from the changes of B-B bonds at the edge of B₃₆ nanocluster. The B-B bonds are elongated/shorten from 1.578/1.686 Å in pristine B₃₆ nanocluster to 1.668/1.683 Å in B₃₆/SA configuration, respectively (see Fig. 3a). Also, S-O bond of SA molecule is elongated from 1.444 Å to 1.524 Å after adsorption at the edge of B₃₆ nanocluster. The obtained charge polarization transfer, changes of enthalpies (ΔH_{ads}) and Gibbs free energies (ΔG_{ads}) of these configurations are calculated and listed in Table 2 and S2. These results also confirm the strong physisorption of SA on the surface of B₃₆

nanocluster in B₃₆/SA configuration. The calculated NBO charge indicates that remarkable charge polarization transfer (388 |me|) occurs from SA to B₃₆ nanocluster, implying the electrostatic interaction between SA and B₃₆ nanocluster. Indeed, the SA molecule acts as a Lewis acid; whereas the nanocluster plays the role of a Lewis base. Actually, the dipole moments of the considered systems in gas phase, which are important since the B₃₆ may be used for a carrier of drugs in biological systems, are also reported in Table 2. The polarity of isolated the B₃₆ and SA molecule is found to be 2.63 and 4.85 Debye, respectively. On the other hand, the high polarity is estimated for the B₃₆/SA configuration about 7.09 Debye. This result indicates that this B₃₆/SA configuration could be solubilized or dispersed in polar mediums, like water. These features and the high polarity recommend that this system is promising candidate for drug delivery because of their high solubility.

A visualization analysis of the non-covalent interactions was made to understand the nature of non-bonding interactions in B₃₆/SA configuration. According to Yang et al., large negative values of sign (λ^2) ρ in the two dimensional RDG plots represent attractive interactions (e.g., hydrogen bonding) whereas large positive values of sign (λ^2) ρ show steric repulsion. On the other hand, the values close to zero (in the low density region) represent van der Waals interaction. Scatter graph of B₃₆/SA configuration in gas phase, illustrated in Fig. 3c, shows that there are several spikes for B₃₆/SA configuration (see Fig. 3c). In each region, more scatter points display larger electron density, that is, larger contribution to total weak interactions. According to Fig. 3c, disperse spikes near sign (λ^2) ρ = -0.01 a.u. can be settled within the regions of the isosurface with deep blue equivalent to stabilizing interactions, viz., O-B, reflective attractions. While, a red space corresponding to the scatter plots with more than -0.01 a.u. for sign (λ^2) ρ indicates a weak repulsive interaction between the SA molecule and B atom at the edge of B₃₆ nanocluster.

This section shows how perturbation in the electronic properties can be an important aspect of the adsorption process. We study the effects of SA molecular adsorption on the electronic properties of the B₃₆ nanocluster in gas phase (see Table 1 and S1). Looking at the results of Table S1, we can see that the energy gap values of A-G configurations remain invariant and no distinct change of E_g is observed by the SA adsorption for these configurations. The percentage of energy gap variation (% Δ E_g) decrease in the range of 0.16% to 1.13%. Therefore, it seems that the SA molecule just floats on the surface of

nanocluster and there is no evidence for chemisorptions or strong physisorptions of this molecule. On the other hand, through the adsorption process of SA at the edge of B₃₆ nanocluster, the energy gap of the B₃₆/SA configuration is found to be 3.15 eV. Based on the HOMO, LUMO, and TDOS visualizations for B₃₆/SA configuration (presented in Fig. 3b), HOMO is more located on nanocluster in B₃₆/SA configuration and slightly on SA molecule, while LUMO in this interacting system is remained over the B₃₆ nanocluster. Table 1 also confirms that the adsorption of SA molecule is accompanied by a significant change near the valance and conduction level compared with pristine B₃₆. In addition, the band gap of the B₃₆/SA configuration decreases by 8.09%, and consequently, the conductivity of the system were changed. Based on reported results, nanocluster can be sensitive enough to sense of SA molecule.

Stable configurations for the interacting system in the gas phase, obtained from previous sections, are reoptimized using PCM with dielectric constant of 78.3553 for water (see Fig. 4a and S2). In these configurations, interaction distance between the SA molecule and surface of B₃₆ nanocluster is about 1.5-3.5 Å. The range of calculated E_{ads} value for these configurations is between -22.31 to -64.62 kJ/mol (see Table 2 and S4). This result reveals that SA molecule is physisorption onto B₃₆ nanocluster in water medium. Like the gas phase, we can see from Table 2 and S4, only B₃₆/SA configuration adsorbed B atom at the edge of B₃₆ nanocluster throughout strong physisorption with E_g equal -64.62 kJ/mol. In this configuration, interaction distance between O atom of sulfonamide and B atom of nanocluster is 1.502 Å which is shorter than in gas phase. It should be noted, the adsorption process leads to a local structural deformation in both fragments. The deformation is obviously seen from the changes of B-B bonds at the edge of B₃₆ nanocluster. The B-B bonds are elongated from 1.578 and 1.685 Å in pristine B₃₆ nanocluster to 1.67 and 1.686 Å in B₃₆/SA configuration, respectively (see Fig. 4a). Also, S-O bond of SA molecule is elongated from 1.444 Å to 1.524 Å after adsorption at the edge of B₃₆ nanocluster. On the other hand, in A-G configurations, SA molecule adsorbed on the both convex and concave surfaces of the B₃₆ nanocluster through weakly physisorption process (see Fig. S2 and Table S4). Therefore, these configurations aren't interested.

The calculated NBO charges indicate that the charge polarization transfer of 425 |me| is occurred from SA molecule to B₃₆ nanocluster, confirming strong physisorption. The main

interaction between the B₃₆ nanocluster and SA in water medium is due to charge transfer from the lone pair orbital of the O atom in SA to the empty p orbital over the B atom of the nanocluster. Hence, SA molecule acts as Lewis acid; in contrast the nanocluster plays the role of a Lewis base. Moreover, the calculated dipole moment for this configuration achieved about 12.98 Debye in contrast 4.10 and 6.31 for isolated B₃₆ and SA molecule, respectively, in water medium. These results indicate that this configuration could be solubilized or dispersed in polar mediums, like water. These features and the high polarity recommend that these systems are promising candidate for drug delivery because of their high solubility.

RDG scatter graph of in B₃₆/SA configuration in water medium is shown in Fig. 4c. The spikes with values near 0.01 a.u. arise from the relatively strong interaction between the oxygen atom in the SA molecule and B atom at the edge of B₃₆ nanocluster. In addition, the spikes with values near -0.01 a.u. arise from the weak repulsive interaction between the SA and B₃₆ nanocluster.

Upon the adsorption process in water medium, E_g of B₃₆/SA configuration is found to be 3.16 eV. The HOMO, LUMO and TDOS calculations are also performed for this configuration, Fig. 4b. According to this figure, the HOMO is located more on nanocluster and slightly over SA molecule in the B₃₆/SA configuration while the LUMO is remained on the nanocluster. It can be seen that after adsorption process in water medium, the valance level and conduction level are closed together compared to that of the pristine B₃₆. These alterations occur closed to the Fermi energy, and therefore can alter the electronic properties of B₃₆. For this reason, the band gap of the B₃₆/SA configuration shows 7.73% decrement, and the conductivity of the system is changed. Based on the mention results, this nanocluster is sensitive enough for adsorption and sensing of SA molecule.

In the end, based on the DFT calculations, we have found that the electronic properties of B₃₆ nanocluster interacting with SA molecule are changed significantly. Our study indicates that the adsorption energy of SA in the exothermic process is negative. Also, based on achieved results, B atom at the edge of B₃₆ nanocluster is the best position for adsorb SA molecule. The reported results in the previous study for the adsorption of fluorouracil molecule on the B₃₆ nanocluster are in consistence with the present results [40]. Therefore, B₃₆ nanocluster is proposed a promising candidate for drug delivery.

Conclusion

In the present research, DFT calculations are performed to scrutinize the interactions between sulfonamide and B₃₆ nanocluster. It is found that the SA molecule remarkably tends to adsorb via its oxygen atoms at the edge of B₃₆ nanocluster with appreciable adsorption energy. The results illustrate that the edge B atoms are more reactive than the inner atoms toward the SA molecule. Indeed, the SA interaction via this nanocluster affected its electronic nature. The energy gaps of the most stable configuration in gas phase reduce by 8.09%. The B₃₆/SA systems are also investigated in water medium. The electrical conductance of B₃₆ is affected via interaction between B₃₆ and sulfonamide in water medium. These features and the high polarity recommend that these systems are promising candidate for drug delivery. Thereby, this system might be an innovative candidate as nanovehicle in nanomedicine domain, which is due to its solubility in water medium. The results might open a new perspective for designing novel drug delivery systems based on boron based nanomaterials.

References

1. Baron S (1996) Protozoa: Structure, Classification, Growth, and Development--Medical Microbiology. University of Texas Medical Branch at Galveston,
2. VanMeter KC, Hubert RJ (2015) Microbiology for the Healthcare Professional-E-Book. Elsevier Health Sciences,
3. Tačić A, Nikolić V, Nikolić L, Savić I (2017) Antimicrobial sulfonamide drugs. *Advanced Technologies* 6 (1):58-71
4. Zoumpoulakis P, Camoutsis C, Pairas G, Soković M, Glamočlija J, Potamitis C, Pitsas A (2012) Synthesis of novel sulfonamide-1, 2, 4-triazoles, 1, 3, 4-thiadiazoles and 1, 3, 4-oxadiazoles, as potential antibacterial and antifungal agents. Biological evaluation and conformational analysis studies. *Bioorganic & medicinal chemistry* 20 (4):1569-1583
5. Ezabadi IR, Camoutsis C, Zoumpoulakis P, Geronikaki A, Soković M, Glamočlija J, Ćirić A (2008) Sulfonamide-1, 2, 4-triazole derivatives as antifungal and antibacterial agents: Synthesis, biological evaluation, lipophilicity, and conformational studies. *Bioorganic & medicinal chemistry* 16 (3):1150-1161
6. Supuran CT, Scozzafava A, Casini A (2003) Carbonic anhydrase inhibitors. *Medicinal research reviews* 23 (2):146-189
7. Supuran CT, Briganti F, Tilli S, Chegwiddden WR, Scozzafava A (2001) Carbonic anhydrase inhibitors: sulfonamides as antitumor agents? *Bioorganic & medicinal chemistry* 9

(3):703-714

8. Shoaib Ahmad Shah S, Rivera G, Ashfaq M (2013) Recent advances in medicinal chemistry of sulfonamides. Rational design as anti-tumoral, anti-bacterial and anti-inflammatory agents. *Mini reviews in medicinal chemistry* 13 (1):70-86
9. Farag AA, Abd-Alrahman SN, Ahmed GF, Ammar RM, Ammar YA, Abbas SY (2012) Synthesis of some azoles incorporating a sulfonamide moiety as anticonvulsant agents. *Archiv der Pharmazie* 345 (9):703-712
10. Tang X, Huang L, Qi C, Wu X, Wu W, Jiang H (2013) Copper-catalyzed sulfonamides formation from sodium sulfinates and amines. *Chemical communications* 49 (54):6102-6104
11. Supuran CT, Casini A, Scozzafava A (2003) Protease inhibitors of the sulfonamide type: anticancer, antiinflammatory, and antiviral agents. *Medicinal Research Reviews* 23 (5):535-558
12. Rendell M (2004) The role of sulphonylureas in the management of type 2 diabetes mellitus. *Drugs* 64 (12):1339-1358
13. Scozzafava A, Mastrolorenzo A, Supuran C (2002) Sulfonamides and sulfonylated derivatives as anticancer agents. *Current Cancer Drug Targets* 2 (1):55-75
14. Fukuoka K, Usuda J, Iwamoto Y, Fukumoto H, Nakamura T, Yoneda T, Narita N, Saijo N, Nishio K (2001) Mechanisms of action of the novel sulfonamide anticancer agent E7070 on cell cycle progression in human non-small cell lung cancer cells. *Investigational new drugs* 19 (3):219-227
15. Kołaczek A, Fusiarsz I, Ławecka J, Branowska D (2014) Biological activity and synthesis of sulfonamide derivatives: a brief review. *Chemik* 68 (7):620-628
16. De Jong WH, Borm PJ (2008) Drug delivery and nanoparticles: applications and hazards. *International journal of nanomedicine* 3 (2):133
17. Ciofani G, Mattoli V (2016) Boron Nitride Nanotubes in Nanomedicine. William Andrew,
18. Wong SS, Joselevich E, Woolley AT, Cheung CL, Lieber CM (1998) Covalently functionalized nanotubes as nanometre-sized probes in chemistry and biology. *Nature* 394 (6688):52
19. Chen X, Kis A, Zettl A, Bertozzi CR (2007) A cell nanoinjector based on carbon nanotubes. *Proceedings of the National Academy of Sciences* 104 (20):8218-8222
20. Zare K, Shadmani N, Pournamdari E (2013) DFT/NBO study of Nanotube and Calixarene with anti-cancer drug. *Journal of Nanostructure in Chemistry* 3 (1):75
21. Farmanzadeh D, Ghazanfary S (2014) DFT studies of functionalized zigzag and armchair boron nitride nanotubes as nanovectors for drug delivery of collagen amino acids. *Struct Chem* 25 (1):293-300

22. Bashiri S, Vessally E, Bekhradnia A, Hosseinian A, Edjlali L (2017) Utility of extrinsic [60] fullerenes as work function type sensors for amphetamine drug detection: DFT studies. *Vacuum* 136:156-162
23. Novoselov KS, Geim AK, Morozov SV, Jiang D, Zhang Y, Dubonos SV, Grigorieva IV, Firsov AA (2004) Electric field effect in atomically thin carbon films. *science* 306 (5696):666-669
24. Iijima S (1991) Helical microtubules of graphitic carbon. *nature* 354 (6348):56
25. Boustani I, Quandt A (1997) Nanotubules of bare boron clusters: Ab initio and density functional study. *EPL (Europhysics Letters)* 39 (5):527
26. Cao L, Zhang Z, Sun L, Gao C, He M, Wang Y, Li Y, Zhang X, Li G, Zhang J (2001) Well-Aligned Boron Nanowire Arrays. *Adv Mater* 13 (22):1701-1704
27. Amsler M, Botti S, Marques MA, Goedecker S (2013) Conducting boron sheets formed by the reconstruction of the α -boron (111) surface. *Phys Rev Lett* 111 (13):136101
28. Pauling L (1960) *The Nature of the Chemical Bond*, vol 260. Cornell university press Ithaca, NY,
29. Janotti A, Van de Walle CG (2007) Hydrogen multicentre bonds. *Nat Mater* 6 (1):44
30. Li X, Grubisic A, Stokes ST, Cordes J, Ganteför G, Bowen KH, Kiran B, Willis M, Jena P, Burgert R (2007) Unexpected stability of Al₄H₆: a borane analog? *Science* 315 (5810):356-358
31. Boustani I (1997) New quasi-planar surfaces of bare boron. *Surf Sci* 370 (2-3):355-363
32. Boustani I (2011) Towards novel boron nanostructural materials. *Chemical Modelling: Applications and Theory* 8:1
33. Zhai H-J, Kiran B, Li J, Wang L-S (2003) Hydrocarbon analogues of boron clusters—planarity, aromaticity and antiaromaticity. *Nat Mater* 2 (12):827
34. Zhai HJ, Alexandrova AN, Birch KA, Boldyrev AI, Wang LS (2003) Hepta- and octacoordinate boron in molecular wheels of eight- and nine-atom boron clusters: observation and confirmation. *Angew Chem Int Ed* 42 (48):6004-6008
35. Huang W, Sergeeva AP, Zhai H-J, Averkiev BB, Wang L-S, Boldyrev AI (2010) A concentric planar doubly π -aromatic B₁₉ cluster. *Nat Chem* 2 (3):202
36. Piazza ZA, Hu H-S, Li W-L, Zhao Y-F, Li J, Wang L-S (2014) Planar hexagonal B₃₆ as a potential basis for extended single-atom layer boron sheets. *Nat Commun* 5:3113
37. Kootenaee AS, Ansari G (2016) B₃₆ borophene as an electronic sensor for formaldehyde: quantum chemical analysis. *Physics Letters A* 380 (34):2664-2668
38. Liu C-S, Wang X, Ye X-J, Yan X, Zeng Z (2014) Curvature and ionization-induced reversible hydrogen storage in metalized hexagonal B₃₆. *J Chem Phys* 141 (19):194306

39. Solimannejad M, Kamalinahad S, Shakerzadeh E (2017) Lin@ B36 (n= 1, 2) nanosheet with remarkable electro-optical properties: a DFT study. *J Electron Mater* 46 (7):4420-4425
40. Shakerzadeh E (2017) Quantum chemical assessment of the adsorption behavior of fluorouracil as an anticancer drug on the B36 nanosheet. *J Mol Liq* 240:682-693
41. Zhao Y, Truhlar DG (2008) Density functionals with broad applicability in chemistry. *Acc Chem Res* 41 (2):157-167
42. Zhao Y, Truhlar DG (2007) Size-selective supramolecular chemistry in a hydrocarbon nanoring. *J Am Chem Soc* 129 (27):8440-8442
43. Yang K, Peverati R, Truhlar DG, Valero R (2011) Density functional study of multiplicity-changing valence and Rydberg excitations of p-block elements: Delta self-consistent field, collinear spin-flip time-dependent density functional theory (DFT), and conventional time-dependent DFT. *J Chem Phys* 135 (4):044118
44. Cossi M, Barone V, Mennucci B, Tomasi J (1998) Ab initio study of ionic solutions by a polarizable continuum dielectric model. *Chem Phys Lett* 286 (3):253-260. doi:10.1016/S0009-2614(98)00106-7
45. Barone V, Cossi M, Tomasi J (1998) Geometry optimization of molecular structures in solution by the polarizable continuum model. *J Comput Chem* 19 (4):404-417. doi:10.1002/(SICI)1096-987X(199803)19:4<404::AID-JCC3>3.0.CO;2-W
46. Reed AE, Weinstock RB, Weinhold F (1985) Natural population analysis. *J Chem Phys* 83 (2):735-746. doi:10.1063/1.449486
47. Frisch M, Trucks G, Schlegel H, Scuseria G, Robb M, Cheeseman J, Scalmani G, Barone V, Mennucci B, Petersson G (2009) Gaussian 09 Revision D. 01, 2009. Gaussian Inc Wallingford CT
48. Geerlings P, De Proft F, Langenaeker W (2003) Conceptual density functional theory. *Chem Rev* 103 (5):1793-1874. doi:10.1021/cr990029p
49. O'boyle NM, Tenderholt AL, Langner KM (2008) CcLib: a library for package-independent computational chemistry algorithms. *J Comput Chem* 29 (5):839-845. doi:10.1002/jcc.20823
50. Johnson ER, Keinan S, Mori-Sanchez P, Contreras-Garcia J, Cohen AJ, Yang W (2010) Revealing noncovalent interactions. *J Am Chem Soc* 132 (18):6498-6506
51. Lu T, Chen F (2012) Multiwfn: a multifunctional wavefunction analyzer. *J Comput Chem* 33 (5):580-592. doi:10.1002/jcc.22885

Table 1. Highest occupied molecular orbital (E_{HOMO}), lowest unoccupied orbital (E_{LUMO}), energy gap (E_g), the change of energy gap of nanocluster after adsorption ($\Delta E_g(\%)$) and Fermi level energies (E_F) of calculated for pristine B_{36} and sulfonamide adsorbed on surface of B_{36} in gas phase and water medium.

| Configuration | | E_{HOMO} (eV) | E_{LUMO} (eV) | E_g (eV) | $\Delta E_g(\%)$ | E_F (eV) |
|---------------|--------------|---------------------------|---------------------------|---------------|------------------|---------------|
| Gas | B_{36} | -6.61 | -3.19 | 3.42 | - | -4.90 |
| Phase | B_{36}/ SA | -6.10 | -2.95 | 3.15 | -8.09 | -4.52 |
| Water | B_{36} | -6.47 | -3.04 | 3.43 | - | -4.75 |
| Medium | B_{36}/ SA | -6.05 | -2.89 | 3.16 | -7.73 | -4.47 |

Table 2. Dipole moment, charge polarization transfer from molecule to nanocluster (Q_T) and adsorption energy (E_{ads}) and calculated thermodynamic properties at 298K and 1atm (ΔH_{ads} and ΔG_{ads}) of B_{36} and configurations in gas phase and water medium.

| | Configuration | Dipole moment | Q_T (me) | E_{ads} (kJ/mol) | ΔH_{ads} (kJ/mol) | ΔG_{ads} (kJ/mol) |
|--------|---------------|---------------|------------|--------------------|---------------------------|---------------------------|
| Gas | B_{36} | 2.63 | - | - | - | - |
| Phase | B_{36}/ SA | 7.09 | 388 | -64.74 | -59.26 | -7.80 |
| Water | B_{36} | 4.10 | - | - | - | - |
| Medium | B_{36}/ SA | 12.98 | 425 | -64.62 | - | - |

Figures

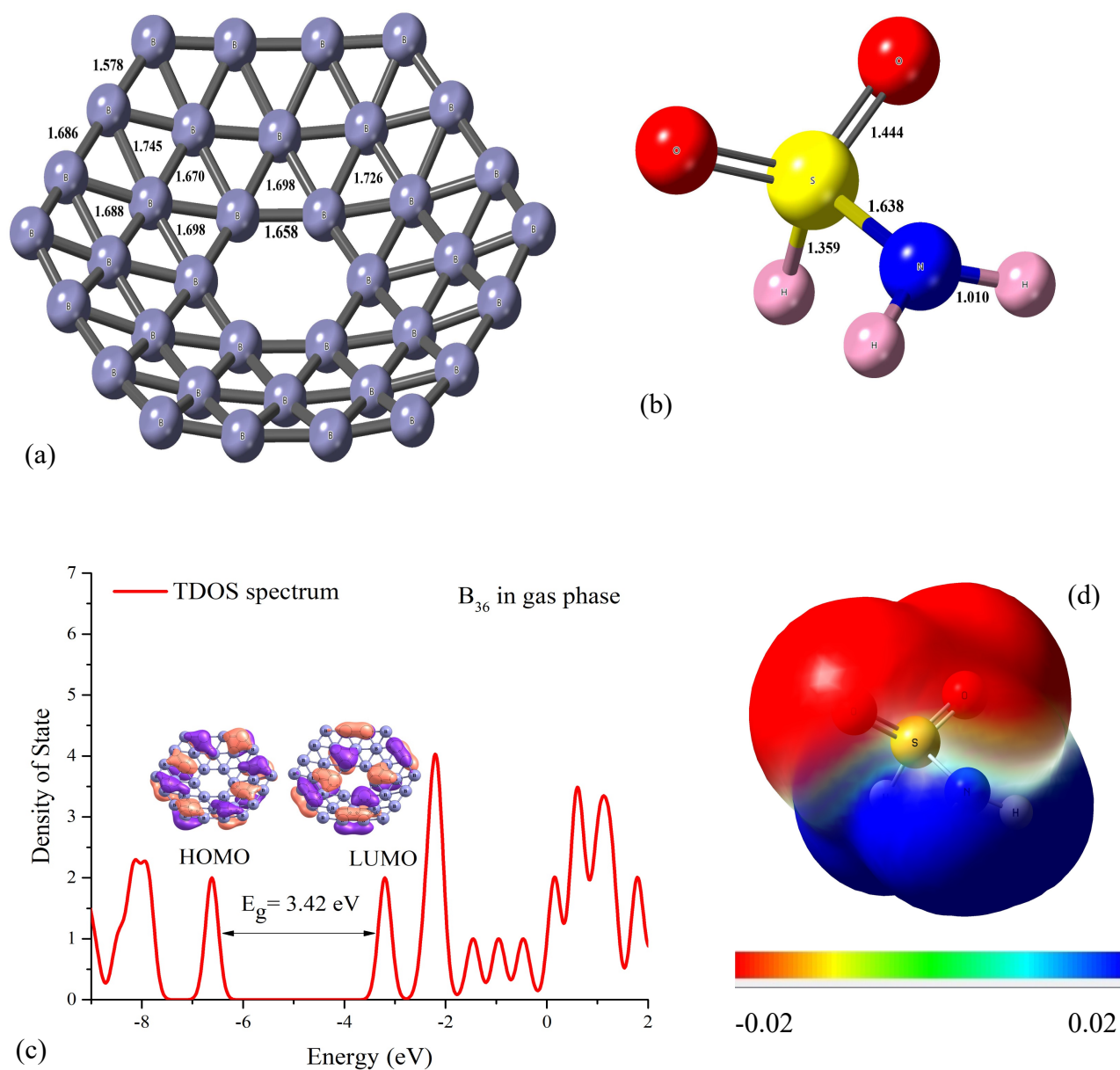


Fig. 1. Optimized structure of (a) B₃₆ (b) sulfonamide, (c) total density of states (TDOS) of B₃₆ in the gas phase and (d) molecular electrostatic potential surface of the sulfonamide. The surfaces are defined by the 0.0004 electrons/b³ contour of the electronic density (All distances are in Å and Color ranges in a.u.).

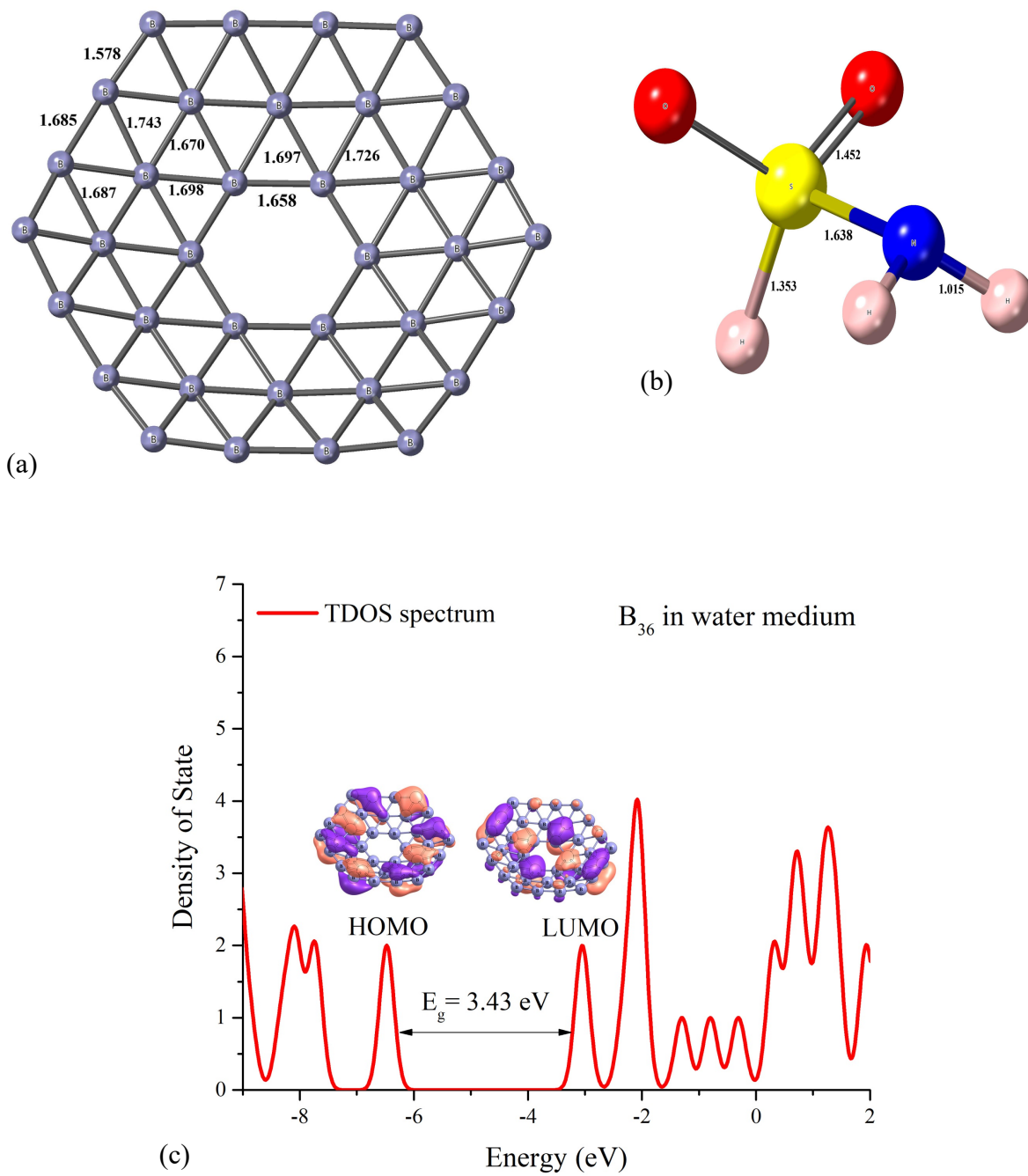


Fig. 2. Optimized structure of (a) pristine B₃₆, (b) sulfonamide and (c) total density of states (TDOS) of pristine B₃₆ in water medium (Bonds in Å).

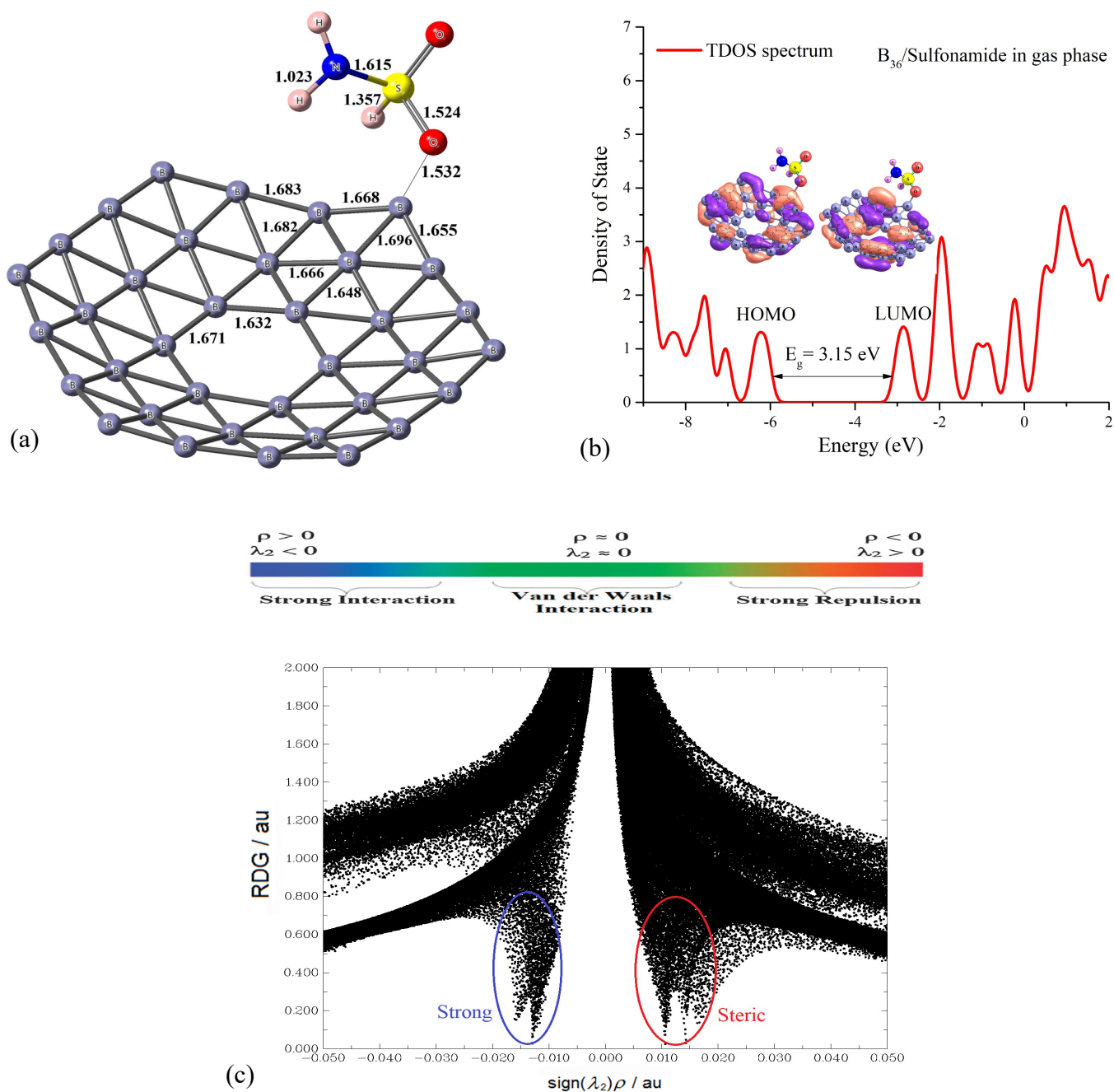


Fig. 3. (a) Optimized structures, (b) total density of states (TDOS) and partial density of states (PDOS) of the B_{36} /Sulfonamide configuration in the gas phase, and (c) plot of the reduced density gradient (RDG) versus $\text{sign}(\lambda_2)\rho$ (isovalue = 0.5 au). (Bonds are in Å).

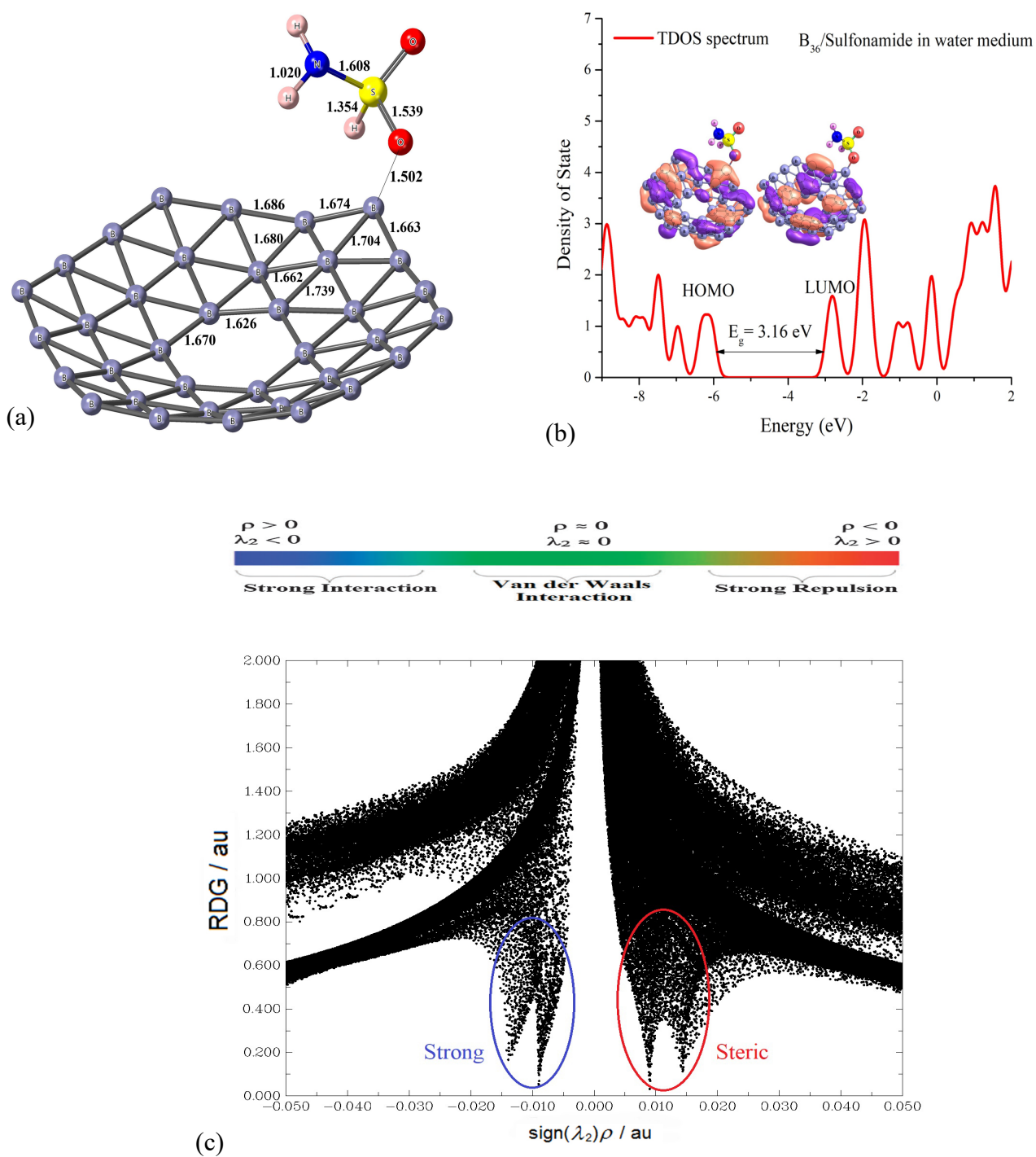


Fig. 4. (a) Optimized structures, (b) total density of states (TDOS) of the B_{36} /Sulfonamide configuration in water medium, and (c) plot of the reduced density gradient (RDG) versus $\text{sign}(\lambda_2)\rho$ (isovalue = 0.5 au). (Bonds are in Å).